

Two-dimensional plasmon induced by metal proximity

V. M. Muravev, P. A. Gusikhin, A. M. Zarezin, I. V. Andreev, S. I. Gubarev, and I. V. Kukushkin
Institute of Solid State Physics, RAS, Chernogolovka, 142432 Russia

 (Received 8 May 2019; published 26 June 2019)

An electromagnetic plasma mode has been discovered in the hybrid system formed by a highly conductive gate strip placed in proximity to the two-dimensional electron system. The plasmon mode propagates along the gate strip with no potential nodes present in transverse direction. Its spectrum combines characteristic features of both gated and ungated two-dimensional plasmons. The plasma excitation has been found to exhibit anomalously strong interaction with light.

DOI: [10.1103/PhysRevB.99.241406](https://doi.org/10.1103/PhysRevB.99.241406)

The problem of electromagnetic waves propagating along metallic wires was treated rigorously by Sommerfeld more than 100 years ago [1]. He demonstrated that plasmon polariton waves travel along the wires at the speed of light. In fact, it is these plasmon polariton waves that carry alternating signals along the modern power lines. Recently, it has been shown theoretically that if a highly conducting wire is placed very close to a much less conducting two-dimensional electron system (2DES), the hybrid system supports a new electromagnetic plasma mode [2]. Remarkably, this proximity plasmon mode differs significantly from both gated and ungated 2D plasma modes that have been known in the literature for over 50 years [3–10]. Its dispersion is described by the following expression:

$$\omega_{\text{pr}}(q) = \sqrt{\frac{2n_s e^2 h q}{m^* \epsilon \epsilon_0 W}} \quad (qW \ll 1), \quad (1)$$

where n_s is the 2D electron density, m^* is the effective electron mass, h is the distance between the gate and 2DES, W is the width of the gate strip, q is the plasmon wave vector directed along the infinite gate, and ϵ is the effective dielectric permittivity of the surrounding medium. Remarkably, the spectrum (1) combines characteristic features of both gated ($\omega_g \propto \sqrt{h}$) and ungated ($\omega_p \propto \sqrt{q}$) plasmons.

In the presence of an external magnetic field, B , normal to the plane of the 2DES, there occurs hybridization between the cyclotron and the plasma motions, which leads to the proximity plasmon magnetodispersion:

$$\omega = \sqrt{\omega_{\text{pr}}^2 + \omega_c^2}, \quad (2)$$

where $\omega_c = eB/m^*$ is the electron cyclotron frequency. It has been shown in [11,12] that in a finite 2DES, two different types of magnetoplasmon modes exist: the cyclotron magnetoplasmon and the one-way edge magnetoplasmon. Importantly, the proximity plasmon excitation does not have the edge magnetoplasmon mode in the presence of a magnetic field. For quantitative treatment of the 2D plasmon mode the reader is referred to Supplemental Material I [13], see Ref. [14].

There are two reasons for which the observation of proximity plasma mode has been hindered over the past 50 years. Foremost, it is due to the fact that proximity plasmon has no charge density nodes in the direction perpendicular to the metal strip, which naturally makes the mode dark to the electromagnetic wave with transversely polarized electric field—a typical configuration used in all pioneering experiments in the field of 2D plasmonics [6–10]. Secondly, the most common geometry considered in theoretical analysis has been that of a finite 2DES with an infinite 2D screening gate [9,15–17]; the configuration which is, in a sense, reciprocal to the one necessary to observe the proximity plasmon. In the presented experiments, we succeeded in making manifest the long lost plasmon excitation.

The experiments were conducted on a single 30-nm-wide GaAs/AlGaAs quantum well structure with electron density in the range of $n_s = (2.2\text{--}2.8) \times 10^{11} \text{ cm}^{-2}$. The quantum well was located at a distance of $h = 4400 \text{ \AA}$ below the crystal surface. Based on the transport measurements, the electron mobility at $T = 1.5 \text{ K}$ was estimated to be $\mu = 5 \times 10^6 \text{ cm}^2/\text{Vs}$. To enable excitation of plasma waves, a metallic gate was lithographically formed on the top surface of the sample, as illustrated by the inset in Fig. 1. The width and the length of the gate for different samples were varied from $W = 20$ to $100 \text{ }\mu\text{m}$ and from $L = 0.5$ to 1.7 mm , respectively. Grounding contacts were fabricated on both sides of the gate, $0.2\text{--}0.4 \text{ mm}$ away from the strip edge. The microwave radiation was guided into the cryostat through a coaxial cable and then coupled to the gate strip by means of a coplanar waveguide transmission line. The microwave frequency was varied in the range of $1\text{--}40 \text{ GHz}$. In order to detect microwave absorption, we employed a noninvasive optical technique [18,19]. The technique is based on the high sensitivity of a recombinant photoluminescence spectrum of 2D electrons to the electron temperature. The photoluminescence spectrum was recorded with and without the excitation microwave radiation and then the absolute value of the difference between the two spectra was integrated over the entire spectral range. Since the resultant integral is directly proportional to the change in the 2D electron temperature, it was used as a measure of microwave absorption. A sample was immersed in a liquid-helium cryostat with

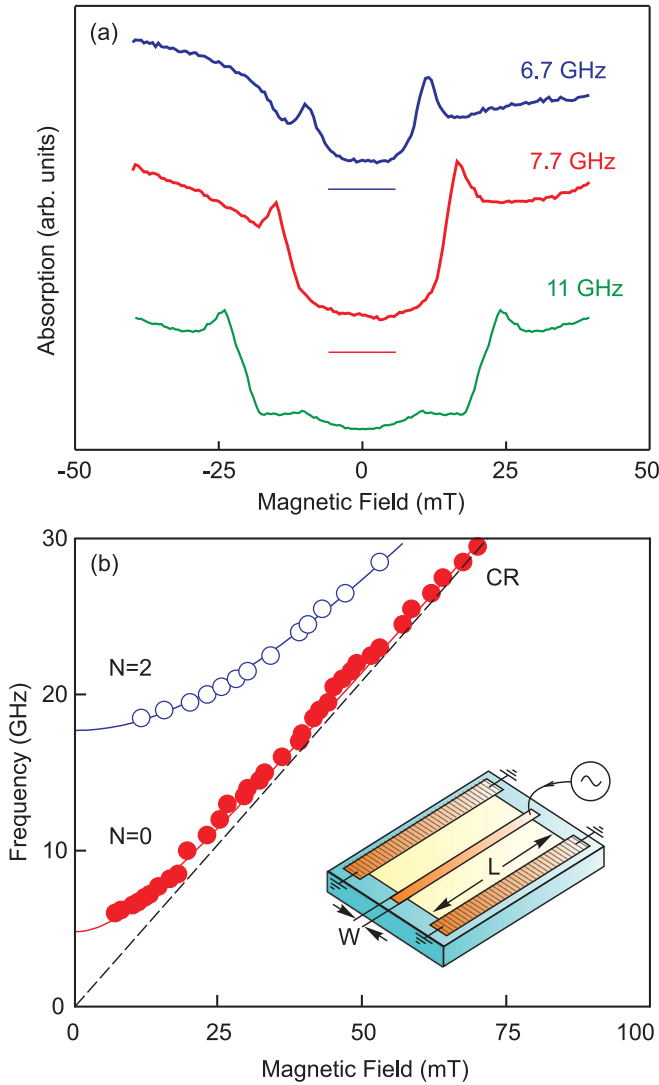


FIG. 1. (a) Dependencies of microwave absorption on magnetic field measured at frequencies of 6.7, 7.7, and 11 GHz. The curves are normalized and offset for the purpose of clarity. Zero signal levels are indicated by short horizontal lines. (b) Magnetodispersion of the proximity plasmon mode with transverse wave numbers $N = 0$ (red circles) and $N = 2$ (empty circles). The theoretical curves calculated for the two modes are plotted with solid red and blue lines, respectively. The inset displays a schematic view of the device with excitation geometry.

superconducting coil. The superconducting coil was used to produce a magnetic field ($B = 0\text{--}2$ T) normal to the sample surface. All the experiments were performed at a temperature of $T = 1.5$ K.

Figure 1(a) illustrates microwave absorption measured in 2DES at 6.7, 7.7, and 11.0 GHz as a function of magnetic field B . For these measurements a structure was used with gate strip dimensions $L = 0.5$ mm and $W = 0.1$ mm, and the 2D electron density, $n_s = 2.7 \times 10^{11}$ cm $^{-2}$. The plotted data clearly indicate that there exists a pronounced absorption peak at each excitation frequency. The peak exhibits a shift to higher values of magnetic field with microwave frequency increase. It was unexpected to find that the resonance arises at approximately 5 GHz, which is considerably lower than

predicted frequency of a gated plasmon [4]:

$$\omega_g(q) = \sqrt{\frac{n_s e^2 \hbar}{m^* \epsilon \epsilon_0}} q \quad (q\hbar \ll 1). \quad (3)$$

According to Eq. (3), the frequency of the lowest gated plasmon mode with wave vector $q_{tr} = \pi N/W$ ($N = 1$) is equal to 10.4 GHz. Therefore, experimental results presented in Fig. 1(a) demonstrate that we have, in fact, observed a 2D plasma excitation with wave vector $q = \pi/L$ directed along the strip gate with $N = 0$ wave number in the transverse direction (for a detailed treatment of the transverse wave vector quantization the reader is referred to Supplemental Material II [13]).

Figure 1(b) displays the measured magnetodispersion of the proximity plasma mode. The red circles in the figure represent the data for the fundamental longitudinal proximity mode with transverse wave number $N = 0$. This set of data is closely approximated by the quadratic function from Eq. (2) plotted with a red line. In the strong magnetic-field limit, the data tends to the cyclotron frequency asymptote (CR) shown with a dashed line. From the fitted curve, the mode can be extrapolated to yield the plasma frequency at $B = 0$ T, $f_p(0) = 4.8$ GHz. This value is in excellent agreement with the theoretical prediction obtained from Eq. (1) for $q = \pi/L$ and $\epsilon = 7.8$. This value of effective dielectric permittivity is very close to the average of the permittivity of GaAs and that of free space, $\epsilon \approx (1 + \epsilon_{\text{GaAs}})/2$ for $\epsilon_{\text{GaAs}} = 12.8$ and $\epsilon_{\text{vacuum}} = 1$.

Unlike the fundamental $N = 0$ proximity mode, the transverse plasma oscillations have $N \geq 1$ potential nodes across the strip. The spectrum of the transverse modes in the limit of $qW \ll 1$ has been found in [2] as

$$\omega^2 = \omega_g(q_{tr})^2 + \omega_{pr}(q)^2 = \frac{n_s e^2 \hbar}{m^* \epsilon \epsilon_0} \left(q_{tr}^2 + \frac{4}{W} q \right), \quad (4)$$

where $q_{tr} = N\pi/W$ ($N = 1, 2, \dots$) is the transverse and $q = \pi/L$ is the longitudinal components of the wave vector. Furthermore, in the long-wavelength limit of $qW \ll 1$, the expression in Eq. (4) reduces to an ordinary form describing a gated plasmon mode, Eq. (3). It is this mode that has been observed in numerous experiments [20–23], whereas the very fundamental plasma excitation with $N = 0$ has been overlooked.

In addition to the fundamental mode, Fig. 1(b) includes measured dispersion data for the transverse proximity plasma mode with $N = 2$ denoted by empty circles. Importantly, due to the symmetric geometry of the E field within the coplanar waveguide, used as an excitation feed, only the modes with even wave number, $N = 2, 4, \dots$, can be excited in the given setup. As shown in the figure, the data can be extrapolated to estimate the mode frequency at $B = 0$ T to be 18 GHz. The theoretical prediction for the transverse wave number, $N = 2$, based on Eq. (4) with $\epsilon = \epsilon_{\text{GaAs}} = 12.8$, is found to be 21 GHz. Such a minor discrepancy between experiment and the theoretical prediction can likely be ascribed to an inaccurate description of the 2DES dielectric environment.

The most significant and remarkable feature of the discovered proximity plasmon mode is its square-root dispersion [2]. This is counterintuitive, considering that a mode having

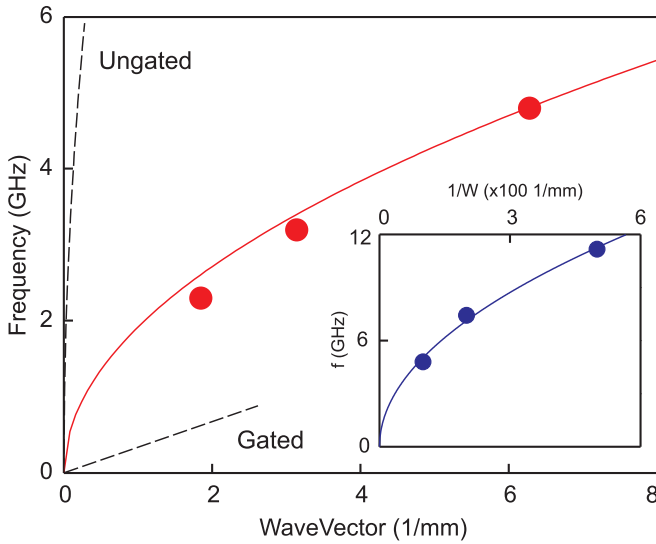


FIG. 2. Proximity plasmon dispersion measured for the gate strip width $W = 100 \mu\text{m}$, gate strip length $L = 0.5, 1.0,$ and 1.7 mm , and electron density $n_s = 2.7 \times 10^{11} \text{ cm}^{-2}$. The theoretical curve is plotted with a solid red line. For comparison, the calculated dispersion of ordinary gated and ungated 2D plasmons is indicated by dashed lines. The inset shows the dependence of plasmon frequency on $1/W$ with blue circles and a solid line denoting measured and calculated data, respectively.

one-dimensional nature emerges in a gated 2DES system. It would be expected that both of these factors should favor linear dispersion law [21,24]. In order to test the theory, the actual dispersion was measured for three samples of different strip length, $L = 0.5, 1.0,$ and 1.7 mm and fixed gate width, $W = 100 \mu\text{m}$. Figure 2 displays the resultant experimental data, designated by red circles, along with the curve calculated using Eq. (1), plotted with a solid red line. It is evident from the figure that experimental results confirm the theoretical prediction of the square-root dispersion. The inset to Fig. 2 shows the measured proximity plasmon frequency as a function of parameter $1/W$, in which case the measurements were performed on three samples of different gate width, $W = 100, 50,$ and $20 \mu\text{m}$ and fixed gate length, $L = 0.5 \text{ mm}$. According to Eq. (1), ω_{pr} is linearly proportional to $1/\sqrt{W}$. Indeed, the obtained data are clearly in close agreement with the theoretical curve plotted with solid blue line.

Concerning the experimental results in Fig. 2, it is worth noting that for the greatest gate strip length, $L = 1.7 \text{ mm}$, the measured data shows a slight deviation from the square-root dispersion of approximately $\Delta\omega/\omega_{\text{pr}} = 10\%$. Such a reduction in plasmon resonant frequency for small wave vector values is a clear indication of hybridization between the plasma waves and the light. However, the magnitude of the observed hybridization far exceeds the level expected of the ordinary 2D plasmons [25–27]. According to theory for the ungated 2D plasmon, $\Delta\omega/\omega_p \approx A^2/4$, where A is a dimensionless retardation parameter defined as the ratio of the plasmon frequency to that of light, given the same wave vector $q = \pi/L$ [27]. In essence, this parameter indicates the influence of the retardation effect. For the proximity plasmon mode under consideration, with $L = 1.7 \text{ mm}, W = 100 \mu\text{m}$,

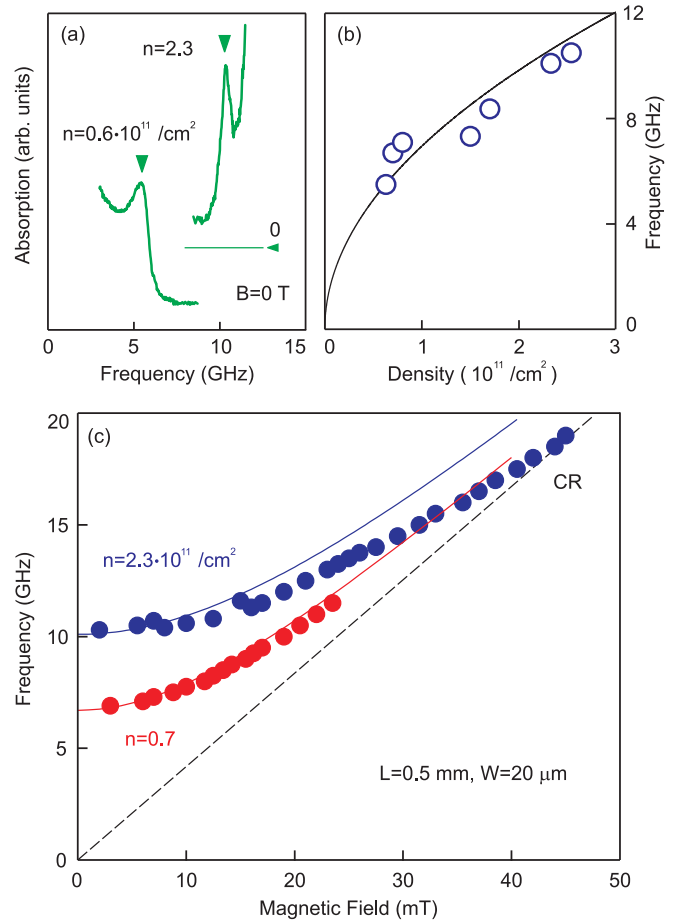


FIG. 3. (a) Microwave absorption spectra measured at $B = 0 \text{ T}$ for electron concentrations of $n_s = 0.6 \times 10^{11} \text{ cm}^{-2}$ and $2.3 \times 10^{11} \text{ cm}^{-2}$. The traces are offset for clarity. (b) Proximity plasmon frequency versus 2D electron density. An overlay plot of the measured data (empty circles) and the calculated curve (solid line). (c) Magnetodispersion for electron densities $n_s = 0.7 \times 10^{11} \text{ cm}^{-2}$ and $2.3 \times 10^{11} \text{ cm}^{-2}$ with theoretical curves denoted by solid red and blue lines.

$n_s = 2.7 \times 10^{11} \text{ cm}^{-2}$, $A = 0.1$ which yields $\Delta\omega/\omega_{\text{pr}} \approx 2.5 \times 10^{-3}$. Remarkably, the degree of coupling determined for the proximity plasmon experimentally is, in fact, 40 times greater than that for the ungated 2D plasmon [25–27].

One of the most attractive properties of 2D plasmons is their tunability. In our experiments, we were able to tune the 2D electron density in the given structure using a photo-depletion method [28]. Figure 3 presents experimental results obtained for the sample with gate dimensions of $W = 20 \mu\text{m}$ and $L = 0.5 \text{ mm}$. The spectral data in Fig. 3(a) illustrates that with a decrease in electron concentration from $n_s = 2.3 \times 10^{11} \text{ cm}^{-2}$ to $0.6 \times 10^{11} \text{ cm}^{-2}$, the resonance peak shifts to the lower frequency. A more detailed dependence of the plasmon frequency on carrier density is shown in Fig. 3(b), where the measured data is compared against the theoretical curve that describes square-root dependence according to Eq. (1). The measured and calculated data, plotted with circles and a solid line, respectively, show excellent agreement between experimental results and theory, demonstrating the possibility

of tuning the speed of the proximity plasma mode over a wide range.

Figure 3(c) displays the dependence of the proximity plasma mode frequency on magnetic field. The measurements were performed for the electron density of $n_s = 0.7 \times 10^{11} \text{ cm}^{-2}$ (red circles) and $2.3 \times 10^{11} \text{ cm}^{-2}$ (blue circles). Experimental data is compared to the theoretical Pythagoras-like law (2), $\omega^2 = \omega_p^2 + \omega_c^2$ (solid lines). We observe that in the high-density limit of $n_s = 2.3 \times 10^{11} \text{ cm}^{-2}$ the magnetoplasma mode intersects the cyclotron resonance line. This again suggests the importance of the retardation effects, viz., strong plasmon-photon coupling. Note that there was observed no influence of retardation effects on the proximity plasmon spectrum obtained for the sample with the same gate strip length, $L = 0.5 \text{ mm}$, but five times greater width, $W = 0.1 \text{ mm}$, as shown in Fig. 1(b). Therefore, the gate width appears to be an additional parameter controlling retardation for the novel proximity plasmon excitation. Found behavior differs dramatically from the coupling of light to the gated and ungated 2D plasmons. In fact, for gated 2D plasmons retardation effects are significantly suppressed and usually not observed at all [29], whereas for ordinary ungated 2D plasmons retardation is dictated by only two parameters: the electron density and the sample size [25–27].

Notably, the overall structural geometry under consideration bears very close resemblance to that of a high-electron mobility transistor (HEMT). It has been shown that plasma oscillations in HEMT structures can be used for detection and generation of the terahertz radiation [30–32], which is based on the idea of compressing the incident radiation into highly confined two-dimensional plasmons propagating in the transistor channel and then rectifying the induced ac potential

within the same device. However, despite the decades-long experimental efforts, terahertz (THz) plasmonic components are still far from their practical realization. Hopefully, the discovery of the proximity plasma mode that exists in the HEMT device geometry may open new avenues for research in the field of terahertz electronics. Indeed, for typical HEMT parameters $L = 10 \text{ }\mu\text{m}$, $W = h = 0.2 \text{ }\mu\text{m}$, and $n_s = 10^{12} \text{ cm}^{-2}$ the proximity plasmon frequency is $f_{\text{pr}} \approx 0.7 \text{ THz}$.

In summary, we have discovered and experimentally investigated a 2D plasma excitation originating in the hybrid system formed by a metallic gate placed in close proximity to the 2DES. The spectrum of the proximity plasmon excitation exhibits features of both gated ($\omega_g \propto \sqrt{h}$) and ungated ($\omega_p \propto \sqrt{q}$) 2D plasmons. Importantly, the observed plasmon mode has a wave vector along the gate strip and no potential nodes present in the transverse direction. Therefore, the peculiar topology of the mode has rendered its detection impossible thus far because it cannot be excited with a transversely polarized E field—the common approach used in all pioneering experiments in 2D plasmonics. Furthermore, we have discovered that the plasma excitation has an anomalously strong interaction with light. This unique property makes the current discovery very promising for the development of THz sensing devices. In addition, being directly applicable to HEMT technology, it can lead to significant progress in developing practical plasmonic components in microwave and terahertz electronics.

We thank V. A. Volkov and A. A. Zabolotnykh for the stimulating discussions. The authors gratefully acknowledge the financial support from the Russian Science Foundation (Grant No. 18-72-10072).

-
- [1] A. Sommerfeld, *Ann. Phys. (NY)* **303**, 233 (1899).
 [2] A. A. Zabolotnykh and V. A. Volkov, *Phys. Rev. B* **99**, 165304 (2019).
 [3] F. Stern, *Phys. Rev. Lett.* **18**, 546 (1967).
 [4] A. V. Chaplik, *Zh. Eksp. Teor. Fiz.* **62**, 746 (1972) [*Sov. Phys. JETP* **35**, 395 (1972)].
 [5] C. C. Grimes and G. Adams, *Phys. Rev. Lett.* **36**, 145 (1976).
 [6] S. J. Allen, Jr., D. C. Tsui, and R. A. Logan, *Phys. Rev. Lett.* **38**, 980 (1977).
 [7] T. N. Theis, J. P. Kotthaus, and P. J. Stiles, *Solid State Commun.* **24**, 273 (1977).
 [8] U. Mackens, D. Heitmann, L. Prager, J. P. Kotthaus, and W. Beinvogl, *Phys. Rev. Lett.* **53**, 1485 (1984).
 [9] D. C. Glattli, E. Y. Andrei, G. Deville, J. Poitrenaud, and F. I. B. Williams, *Phys. Rev. Lett.* **54**, 1710 (1985).
 [10] T. Demel, D. Heitmann, P. Grambow, and K. Ploog, *Phys. Rev. Lett.* **66**, 2657 (1991).
 [11] S. J. Allen, Jr., H. L. Störmer, and J. C. M. Hwang, *Phys. Rev. B* **28**, 4875 (1983).
 [12] V. A. Volkov and S. A. Mikhailov, *Zh. Eksp. Teor. Fiz.* **94**, 217 (1988) [*Sov. Phys. JETP* **67**, 1639 (1988)].
 [13] See Supplemental Material at <http://link.aps.org/supplemental/10.1103/PhysRevB.99.241406> for the quantitative interpretation of proximity 2D plasma mode and consideration of transverse wave vector quantization.
 [14] G. R. Aizin and G. C. Dyer, *Phys. Rev. B* **86**, 235316 (2012).
 [15] A. L. Fetter, *Phys. Rev. B* **33**, 5221 (1986).
 [16] E. H. Hwang and S. Das Sarma, *Phys. Rev. B* **75**, 205418 (2007).
 [17] V. Ryzhii, A. Satou, and T. Otsuji, *J. Appl. Phys.* **101**, 024509 (2007).
 [18] B. M. Ashkinadze, E. Linder, E. Cohen, and A. Ron, *Phys. Status Solidi A* **164**, 231 (1997).
 [19] I. V. Kukushkin, J. H. Smet, K. von Klitzing, and W. Wegscheider, *Nature (London)* **415**, 409 (2002).
 [20] P. J. Burke, I. B. Spielman, J. P. Eisenstein, L. N. Pfeiffer, and K. W. West, *Appl. Phys. Lett.* **76**, 745 (2000).
 [21] V. M. Muravev, C. Jiang, I. V. Kukushkin, J. H. Smet, V. Umansky, and K. von Klitzing, *Phys. Rev. B* **75**, 193307 (2007).
 [22] W. F. Andress, H. Yoon, K. Y. M. Yeung, L. Qin, K. West, L. Pfeiffer, and D. Ham, *Nano Lett.* **12**, 2272 (2012).
 [23] D. A. Iranzo, S. Nanot, E. J. C. Dias, I. Epstein, C. Peng, D. K. Efetov, M. B. Lundberg, R. Parret, J. Osmond, J.-Y. Hong, J. Kong, D. R. Englund, N. M. R. Peres, and F. H. L. Koppens, *Science* **360**, 291 (2018).
 [24] I. V. Kukushkin, J. H. Smet, V. A. Kovalskii, S. I. Gubarev, K. von Klitzing, and W. Wegscheider, *Phys. Rev. B* **72**, 161317(R) (2005).

- [25] I. V. Kukushkin, J. H. Smet, S. A. Mikhailov, D. V. Kulakovskii, K. von Klitzing, and W. Wegscheider, *Phys. Rev. Lett.* **90**, 156801 (2003).
- [26] I. V. Kukushkin, V. M. Muravev, J. H. Smet, M. Hauser, W. Dietsche, and K. von Klitzing, *Phys. Rev. B* **73**, 113310 (2006).
- [27] P. A. Gusikhin, V. M. Muravev, A. A. Zagitova, and I. V. Kukushkin, *Phys. Rev. Lett.* **121**, 176804 (2018).
- [28] I. V. Kukushkin, K. von Klitzing, K. Ploog, V. E. Kirpichev, and B. N. Shepel, *Phys. Rev. B* **40**, 4179 (1989).
- [29] A. V. Chaplik, *Pis'ma Zh. Eksp. Teor. Fiz.* **101**, 602 (2015) [*JETP Lett.* **101**, 545 (2015)].
- [30] M. Dyakonov and M. Shur, *IEEE Trans. Electron Devices* **43**, 1640 (1996).
- [31] M. S. Shur and V. Ryzhii, *Int. J. High Speed Electron. Syst.* **13**, 575 (2003).
- [32] W. Knap, M. Dyakonov, D. Coquillat, F. Teppe, N. Dyakonova, J. Łusakowski, K. Karpierz, M. Sakowicz, G. Valusis, D. Seliuta, I. Kasalynas, A. El Fatimy, Y. M. Meziani, and T. Otsuji, *J. Infrared Millimeter Terahertz Waves* **30**, 1319 (2009).